Electronic Supplementary Material (ESI) for Physical Chemistry Chemical Physics.

Titanium Nitride-Based Hyperbolic Metamaterial for Near-Infrared Ultrasensitive Sensing of Microbes: ESI

S1. SUGGESTED FABRICATION TECHNIQUE

It is essential to meticulously adopt the fabrication procedure to produce our proposed TiN nanowire HMM structure. We could employ electron beam lithography (EBL) and electroplating techniques to fabricate the TiN nanowire HMM structure. Yan *et al.* fabricated a nanowire HMM structure on the glass-metal hybrid substrate using EBL and electroplating methods [1]. Sahoo *et al.* reported an HMM structure comprising highly packed nanowires (high FF) using sputtering and electroplating methods [2]. Figure S1 illustrates a simplified diagram of the suggested fabrication method for building the proposed nanowire HMM structure. Initially, we could use sputtering or electroplating methods to deposit TiN on PMMA glass to support nanowires. EBL can achieve a well-structured periodic array of holes that can be removed using an etchant such as acetone. After that, we might grow TiN nanowires using the electroplating method. Then, ultraviolet (UV) light can be utilized to soften the PMMA material. Finally, we could use acetone to remove all PMMA materials.

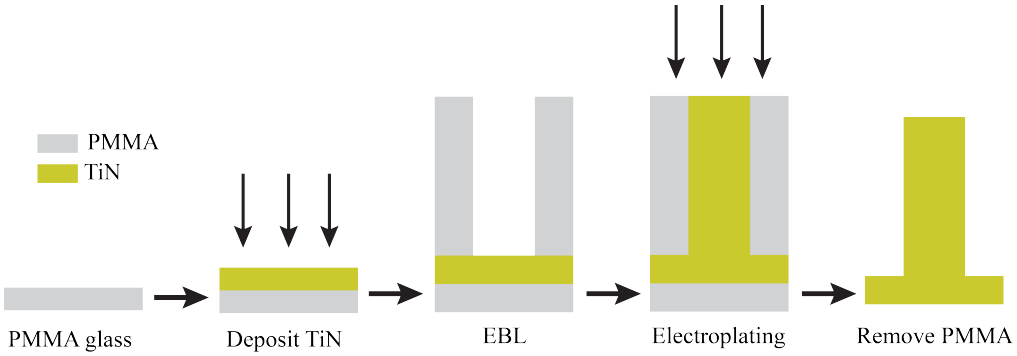

Fig. S1. Suggested fabrication technique of our proposed TiN nanowire HMM sensor structure.

S2. MATERIAL PROPERTIES OF TITANIUM NITRIDE

We adopted the complex refractive index of titanium nitride (TiN) from experimental data of Naik *et al.* [3]. The complex refractive index, $\tilde{n}$, is defined by,

$$\tilde{n} = \mathrm{n} + i\mathrm{k}. \tag{S1}$$

Here, n and k denote the refractive index and extinction coefficient. The n controls the light's speed through the medium, while the k governs its scattering and absorption. The dielectric constants of TiN are given in Fig. S2. The magnetic permeability of the TiN was set to be 1 for our study.

S3. REFLECTANCE, TRANSMITTANCE, AND ABSORPTANCE SPECTRA

To calculate the reflectance (R), transmittance (T), and absorptance (A) of our proposed structure, we utilized two power monitors: one was set below the structure, and the other was set on the

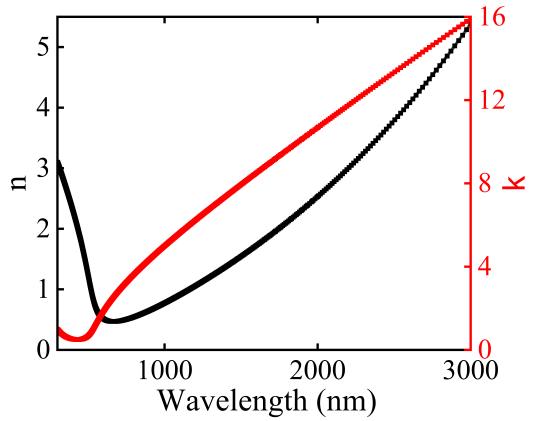

Fig. S2. Refractive index (n) and extinction coefficient (k) spectra of TiN.

top of the incident light. R, T, and A were enumerated by,

$$\mathrm{R} = \frac{P_r}{P_i}, \tag{S2}$$

$$\mathrm{T} = \frac{P_t}{P_i}, \text{ and} \tag{S3}$$

$$\mathrm{A} = 1 - \mathrm{R} - \mathrm{T}. \tag{S4}$$

Here, P_r, P_t, and P_i represent the monitors' reflected, transmitted, and incident power. We obtained two bulk plasmon polariton (BPP) modes at the resonance wavelengths of 1267 and 1935 nm, as shown in Fig. S3, where the water (refractive index, n = 1.333 RIU) was considered as the surrounding medium. Consequently, our proposed hyperbolic metamaterials (HMM) structure exhibited absorptance at the resonance wavelengths, as no transmission through the structure was supported because of maintaining dispersion relations. The effective permittivity, ε, of the proposed HMM structure is negative; therefore, the propagation constant, $k = \sqrt{\varepsilon}\omega$, of the electromagnetic wave is imaginary. Thus, the proposed HMM sensor structure exhibited negligible transmittance.

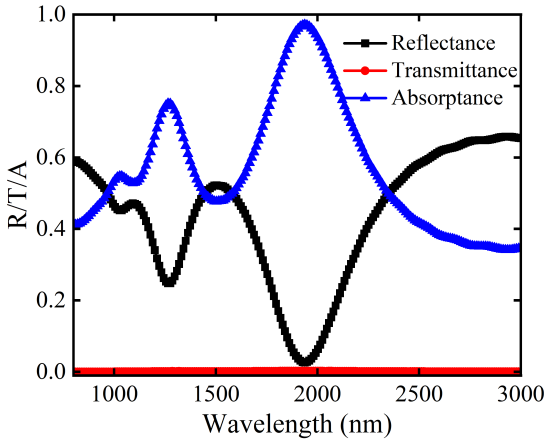

Fig. S3. Reflectance, transmittance, and absorptance spectra of the proposed HMM sensor structure. Here, the fill factor of TiN nanowire was set to be 70%.

S4. EFFECTS OF FILL FACTOR ON REFLECTANCE SPECTRA

We studied the impact of various fill factors, FF, on the reflectance spectra. The BPP modes disappeared while we increased the FF beyond 78.54% because nanowires overlapped each other. We observed it for the FF of 78.54%, as depicted in Fig. S4. Moreover, it can be inferred from Fig. S4 that BPP modes initiated to disappear with increasing FF beyond 70%. Therefore, we considered the 70% FF for our proposed HMM sensor structure.

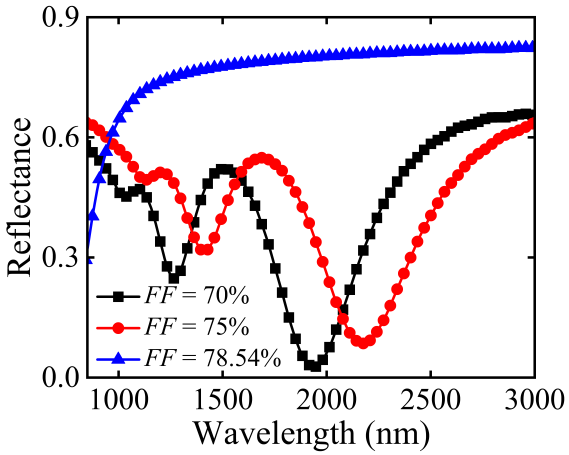

Fig. S4. Reflectance spectra of the nanowire HMM sensor structure for different FF.

S5. MODE FREQUENCY SHIFT FOR DIFFERENT FILL FACTOR

We analyzed the mode frequency shift of the second (q = 2) BPP mode by varying the FF of the TiN nanowire, where other structural parameters were kept the same. An improved mode frequency shift was obtained when we increased the FF, as shown in Fig. S5. Meanwhile, this happened due to strong hyperbolic dispersion, which resulted in the shift of BPP mode in the longer wavelength.

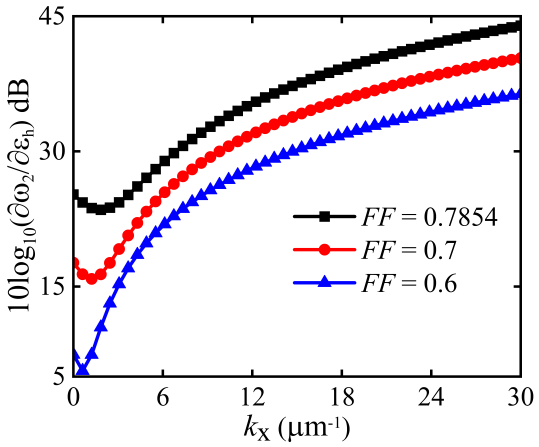

Fig. S5. The calculated mode frequency shift of q = 2 BPP mode for different FF, where h_p was set to be 400 nm.

S6. SENSING CAPABILITIES OF VARIOUS MICROBES

We slightly changed the surrounding medium's RI due to injecting microbes into freshwater solutions. Here, we injected a single *Escherichia coli* (*E. coli*), 4% Dengue infected platelets, and 4% *Haemophilus influenzae* (*H. influenzae*) into freshwater. We collected the RI of single *E. coli* bacteria (difference of RI, Δ = 0.005 RIU) from an experimental report of the optofluidic immersion refractometry technique [4]. The optical properties of Dengue infected platelets (n = 1.39) and *H. influenzae* (n = 1.45) were adopted from Sharma *et al.* [5] and Locke *et al.* [6], respectively. After that, we mixed 4% of Dengue-infected platelets and *H. influenzae* with freshwater and obtained the effective relative complex permittivity, ε_{eff}, of the mixture by solving the Maxwell Garnett equation [7],

$$\varepsilon_{eff} = \varepsilon_w[1 + 3c_m \frac{\varepsilon_m - \varepsilon_w}{\varepsilon_m + 2\varepsilon_w - c_m(\varepsilon_m - \varepsilon_w)}]. \tag{S5}$$

Here, ε_m and ε_w denote the permittivity of the microbe and freshwater. c_m represents the volume fraction of the microbe in freshwater. All the structural and simulation parameters were kept constant.

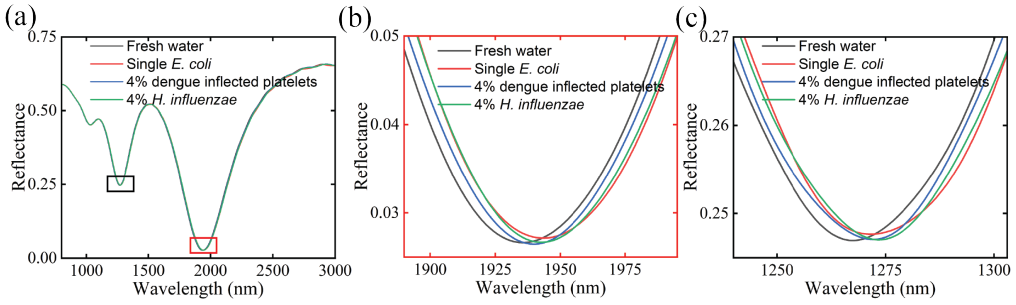

Fig. S6. (a) Reflectance spectra of the proposed nanowire HMM sensor structure by adding different microbe into fresh water. Zoomed view of red-shifted reflectance spectra for (b) q = 1 and (c) q = 2 modes. Red and black rectangular denote the fundamental and second BPP modes, respectively.

The proposed HMM sensor structure redshifted the resonance dips in the reflectance, when we injected a single *E. coli*, 4% Dengue inflected platelets, and 4% *H. influenzae* into freshwater, as depicted in Fig. S6. We compared the reflectance spectra of freshwater and the aqueous solution containing microbes and calculated the resonance wavelength shift. Two BPP modes were redshifted due to the addition of microbes in freshwater. We obtained the resonance wavelength shifts of 11, 5, and 8 nm for q = 1 BPP mode and 5.41, 3.11, and 6 nm for q = 2 BPP mode, respectively, as shown in Figs. S6(b) and (c), for a single *E. coli*, 4% Dengue inflected platelets, and 4% *H. influenzae* into freshwater, respectively. Therefore, it can be inferred that our proposed HMM sensor structure is capable of detecting a small amount of several microbes in freshwater solution.

S7. LIMIT OF DETECTION

We studied the impact of the refractive index difference, Δn, on the resonance shift of the reflectance spectra. The limit of detection (LOD) of our proposed nanowire HMM sensor structure is 0.00008 RIU. Here, we obtained a resonance shift of 0.27 nm for both BPP modes, as shown in Fig. S7. When we reduced Δn, no resonance shifts were achieved in either BPP mode.

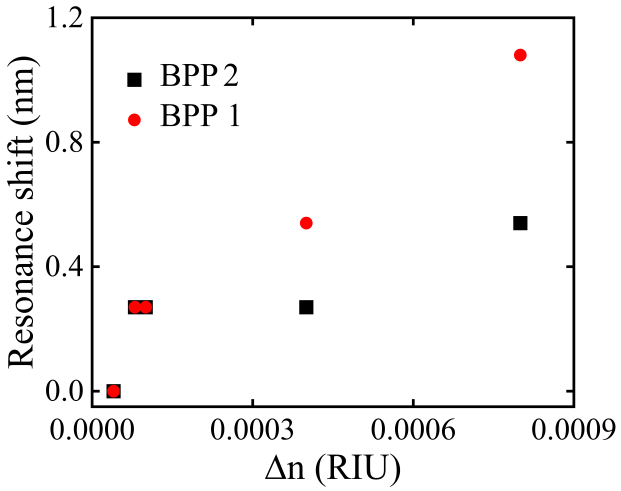

Fig. S7. Resonance wavelength shift of BPP 1 and 2 modes for varying the refractive index difference, Δn. We obtained an LOD of 0.00008 RIU for our proposed HMM sensor structure.

S8. ELECTRIC FIELD DISTRIBUTIONS AROUND NANOWIRE

The resonance wavelength shift exhibited irregular fluctuations with varying D/h_p due to the fluctuations of the electric field around the nanowire. The binding of *E. coli* bacteria with nanowires altered with varying D/h_p, which resulted in the electric field fluctuations for both BPP modes, as shown in Fig. S8. We achieved the highest electric field distributions around the TiN nanowire for BPP 1 mode due to the strong hyperbolic dispersion. Thus, we observed a high resonance wavelength shift for the BPP 1 mode compared to the BPP 2 mode. However, our proposed structure at the D/h_p of 0.5 and 0.6 exhibited a high resonance wavelength shift for the BPP 2 mode because of high electric field distributions around TiN nanowire, as shown in Fig. S8(b).

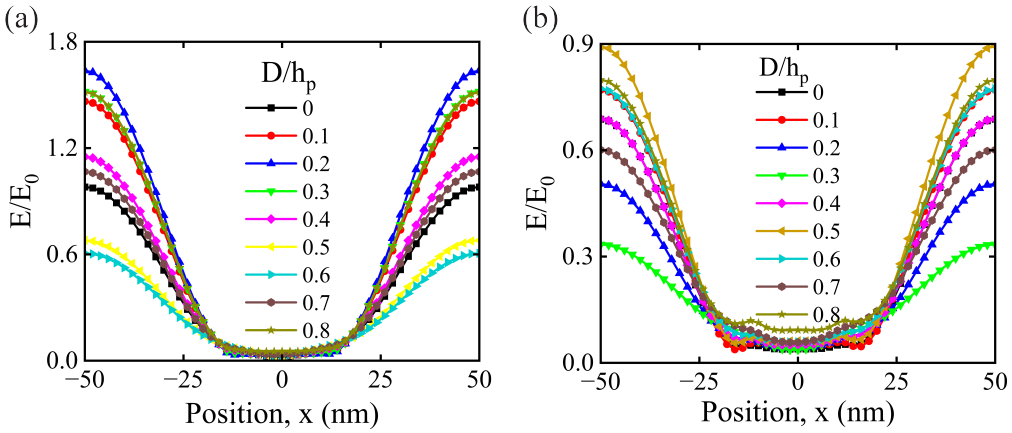

Fig. S8. Normalized electric field distributions of (a) BPP 1 and (b) BPP 2 modes around the TiN nanowire for varying the position of *E. coli* bacteria, D/h_p.

S9. DEPENDENCY OF A SINGLE MICROBE'S POSITION ON RESONANCE SHIFT

We analyzed the effect of a single *E. coli*'s position on the resonance shift of the proposed nanowire HMM sensor structure. We varied the *E. coli*'s position by changing D/h_p in our proposed structure. We obtained different resonance shifts for both BPP modes while we varied the D/h_p, as shown in Fig. S9. Meanwhile, the binding of the microbe with the HMM's nanowire altered

with varying D/h_p. Interestingly, our proposed sensor structure exhibited resonance wavelength shift for the worst cases of D/h_p.

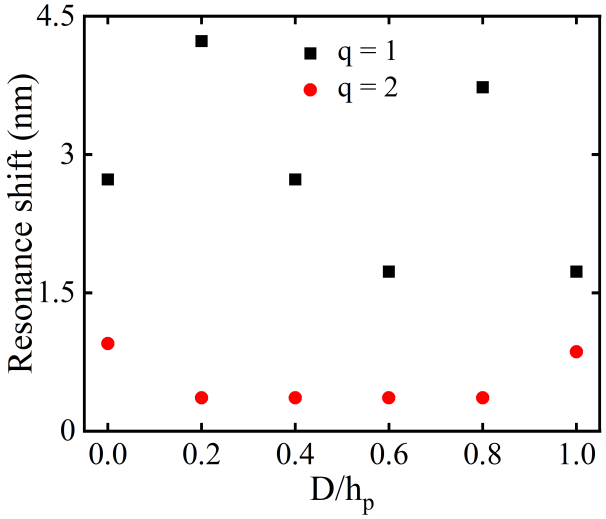

Fig. S9. Numerically calculated resonance shift of dips in reflectance spectra for varying a single *E. coli*'s D/h_p.

REFERENCES

1. R. Yan, T. Wang, X. Yue, *et al.*, "Highly sensitive plasmonic nanorod hyperbolic metamaterial biosensor," Photon. Res. **10**, 84–95 (2022).
2. M. K. Sahoo, A. A. VS, and A. Kumar, "Electroplating-based engineering of plasmonic nanorod metamaterials for biosensing applications," Nanotechnology **34**, 195301 (2023).
3. G. V. Naik, B. Saha, J. Liu, *et al.*, "Epitaxial superlattices with titanium nitride as a plasmonic component for optical hyperbolic metamaterials," Proc. Natl. Acad. Sci. **111**, 7546–7551 (2014).
4. P. Liu, L. Chin, W. Ser, *et al.*, "Real-time measurement of single bacterium's refractive index using optofluidic immersion refractometry," Procedia Eng. **87**, 356–359 (2014). EUROSENSORS 2014, the 28th European Conference on Solid-State Transducers.
5. S. Sharma and A. Kumar, "Design of a biosensor for the detection of dengue virus using 1d photonic crystals," Plasmonics **17**, 675–680 (2022).
6. A. K. Locke, F. R. Zaki, S. T. Fitzgerald, *et al.*, "Differentiation of otitis media-causing bacteria and biofilms via raman spectroscopy and optical coherence tomography," Front. Cell. Infect. Microbiol. **12** (2022).
7. J. C. M. Garnett and J. Larmor, "Xii. colours in metal glasses and in metallic films," Philos. Transactions Royal Soc. London. Ser. A, Containing Pap. a Math. or Phys. Character **203**, 385–420 (1904).